Supporting Information

Synergistic V/S co-doping induces dual-site activation and superhydrophilicity in BiOI for enhanced photocatalytic hydrogen evolution

Xiaojie Luo[1,#], Zhengjie Su[1,#], Haoyu Wang[1,#], Kening Xiang[1], Tao Liu[1], Dong-Hau Kuo[2,*], Hai Huang[1,*], Jinguo Lin[1,*], Xiaoyun Chen[1,*], Jiqing Li[1,*]

[1] College of Materials Engineering, Fujian Agriculture and Forestry University, Fuzhou 350002, China

[2] Department of Materials Science and Engineering, National Taiwan University of Science and Technology, Taipei 106335, Taiwan

# These authors contributed equally to this work.

*Corresponding author

E-mail address: dhkuo@mail.ntust.edu.tw (D. H. Kuo)

E-mail address: 229306303@qq.com (H. Huang)

E-mail address: fjlinjg@126.com (J. Lin)

E-mail address: fjchenxy@126.com (X. Chen)

E-mail address: nfuljq@163.com (J. Li)

CONTENTS

Experimental Section

1. Apparent quantum efficiency computation

According to the literature reports, the apparent quantum efficiency (AQE) is measured [1]. The experiment was conducted under photocatalytic reaction conditions of monochromatic light at 420 nm (λ), an average radiation intensity (I) of 55.72 mW/cm^2, and an irradiation area (A) of 33.92 cm^2. During the PHER experiment, 50 mg of catalyst was added to 50 mL of deionized water (with a conductivity of 15.8 mΩ/cm and a pH of 6.8), along with 10 mmol of Na_2S and 10 mmol of Na_2SO_3 as sacrificial agents. The reactor is then degassed for 30 min using a circulating water-cooling system. An online Panna-A91 GC system with 99.999% purity He as the carrier gas was used to gauge the H_2 generated; the initial and final temperatures of the reaction solution were 25.6 and 26.1 °C, respectively. The total H_2 evolution with 50 mg of V/S-BiOI-3 catalyst was 924.6 μmol after 6 h of reaction, which can be used to determine the reacted photons (N_{reac}). The number of photons (N_{in}) illuminated on the reactor is computed according to the following equations:

$$N_{in} = \frac{E \times \lambda}{h \times c} = \frac{A \times I \times t \times \lambda}{h \times c} = \frac{33.92 \times 55.72 \times 10^{-3} \times 3600 \times 6 \times 420 \times 10^{-9}}{6.626 \times 10^{-34} \times 3 \times 10^{8}} = 8.63 \times 10^{22}$$

$$AQE = \frac{N_{reac}}{N_{in}} \times 100\% = \frac{2 \times 6.02 \times 10^{23} \times 924.6 \times 10^{-6}}{8.63 \times 10^{22}} \times 100\% = 12.9\%$$

2.2 Characterization of V/S-BiOI catalysts

2.2.1 X-ray diffraction (XRD) measurement

The catalyst powder was evenly spread on a glass slide, and an XRD test was conducted using a Rigaku Ultima IV Phaser X-ray diffractometer, operating at a radiation wavelength of 1.5405 Å with a voltage of 40 kV and a current of 40 mA, over a scan range of 10° - 80°.

2.2.2 Field emission scanning electron microscope (FE-SEM) measurement

A small amount of the powder sample was evenly dispersed on conductive carbon tape and sputter-coated with a thin platinum layer under vacuum. The microstructure was then characterized using a Hitachi SU-8010 FE-SEM at an accelerating voltage of 5 kV and a beam current of 10 μA.

2.2.3 Ultraviolet-visible spectroscopy (UV-vis) measurement

The catalyst was adhered to transparent tape to measure its light absorption properties. The UV-Vis diffuse reflectance spectrum was recorded using a Lambda 750S spectrophotometer, referenced against barium sulfate (A.R.). The measurement was conducted with a resolution of 2 cm^{-1} over a wavelength range of 200-2000 nm.

2.2.4 X-ray photoelectron spectroscopy (XPS) measurement

The catalyst powder was pressed into a pellet for XPS analysis. The measurement was conducted under an ultra-high vacuum (5×10^{-9} mbar) using a Thermo Scientific K-Alpha+ spectrometer with a monochromatic Al Kα X-ray source (1486.6 eV). The instrument was operated at 15 kV and 15 mA, and the data were collected in Constant Analyzer Energy (CAE) mode.

2.2.5 Ultraviolet photoelectron spectroscopy (UPS) measurement

The catalyst surface was cleaned by sputtering with Ar ions/clusters and then mounted on a conductive sample holder. The analysis chamber was evacuated to an ultra-high vacuum of 3×10^{-8} mbar. UPS was performed using a Thermo Scientific Nexsa instrument with He I radiation (21.22 eV) as the excitation source. A bias voltage of -5 eV or +10 eV was applied to accurately determine the secondary electron cutoff region. From the acquired data, the work function (φ), secondary electron cutoff energy (E_C), and Fermi level (E_F) were derived.

2.2.6 Specific surface area measurement

The specific surface area (S_{BET}) and pore structure were determined using an ASAP 2000 instrument. The samples were degassed at 105 °C for 6 h before analysis. The surface area was calculated using the Brunauer-Emmett-Teller (BET) formula, and the pore size distribution was evaluated via the Barrett-Joyner-Halenda (BJH) equation.

2.2.7 Fourier transform infrared spectroscopy (FTIR) measurement

Fourier transform infrared (FTIR) analysis was performed using a Nicolet-380 Fourier transform infrared spectrometer, with the catalyst embedded in potassium bromide at a weight ratio of 1:100.

2.2.8 X-ray fluorescence (XRF) spectrometry measurement

X-ray fluorescence (XRF) spectrometry was conducted using a SHIMADZU XRF-1800 apparatus.

2.2.9 Electrochemical measurements

Electrochemical measurements were performed using a Biologic SP-300 potentiostat with a standard three-electrode configuration. The working electrode was prepared by uniformly mixing the catalyst, acetylene black, and polytetrafluoroethylene (PTFE) binder in a mass ratio of 8:1:1. This mixture was coated onto a 1 cm × 1 cm titanium mesh, pressed under 20 MPa for 15 s, and then dried at 85 ^{o}C for 5 h. A Pt wire and an Ag/AgCl electrode served as the counter and reference electrodes, respectively. The electrochemical performance was evaluated in a 1 M Na_2SO_4 aqueous solution (pH = 6.8). Furthermore, the stability of the catalyst was assessed via cyclic voltammetry in an aqueous solution containing 1 M KCl, 5 mM $K_3[Fe(CN)_4]$, and 5 mM $K_4[Fe(CN)_6]$.

2.2.10 Contact angle measurement

Hydrophilicity and hydrophobicity of the samples were evaluated using a DSA 30 contact angle

analyzer. Before measurement, the instrument was calibrated and adjusted to the optimal testing position. The catalyst powders were uniformly loaded and compressed between two glass slides to obtain a flat and compact surface. A droplet of distilled water was then deposited onto the sample surface, and its profile was recorded at regular time intervals. The contact angle was determined using the baseline circle–fitting method. Each measurement was repeated ten times at different positions on the sample surface, and the average value was reported.

2. Additional Figures

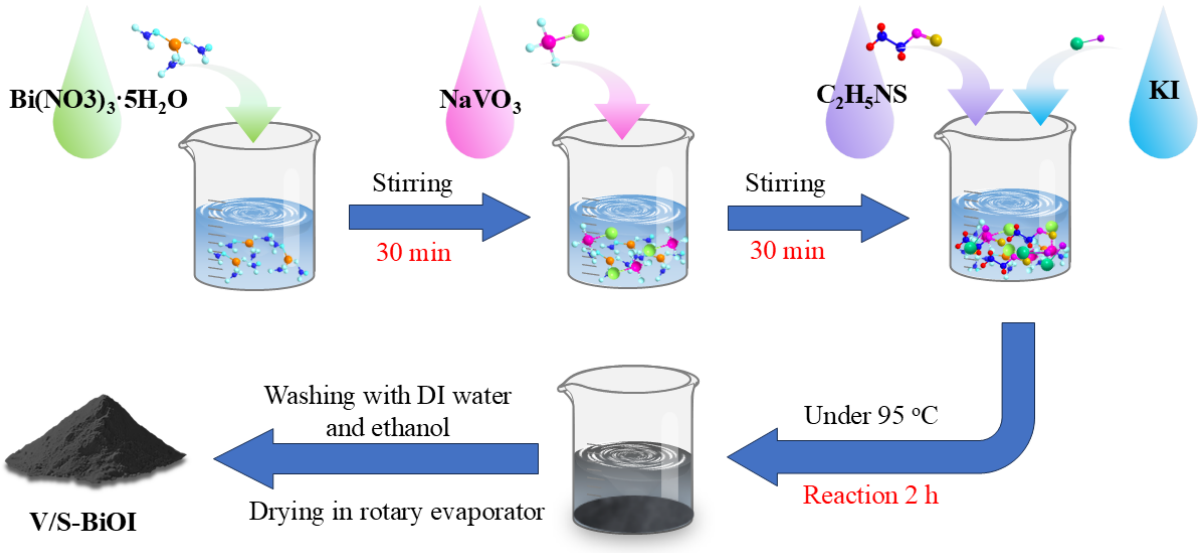

Fig. S1 Schematic representation of the synthesis of V/S-BiOI catalysts.

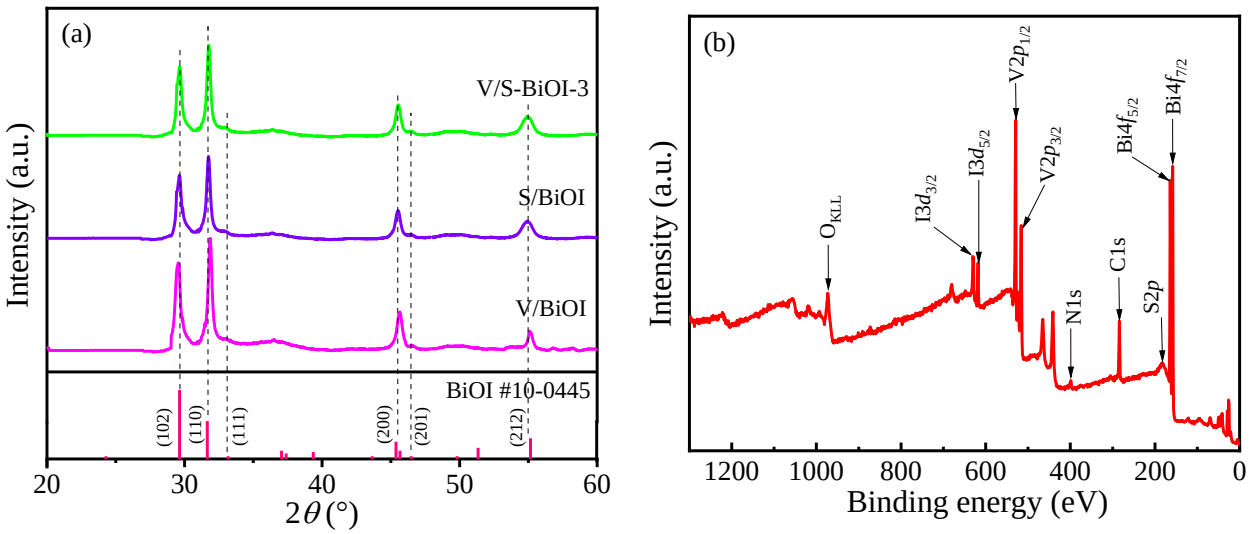

Fig. S2 (a) XRD patterns of V/S-BiOI-3, S/BiOI, V/BiOI, and the standards of BiOI (PDF#10–0445).

(b) The XPS survey spectrum of V/S-BiOI-3.

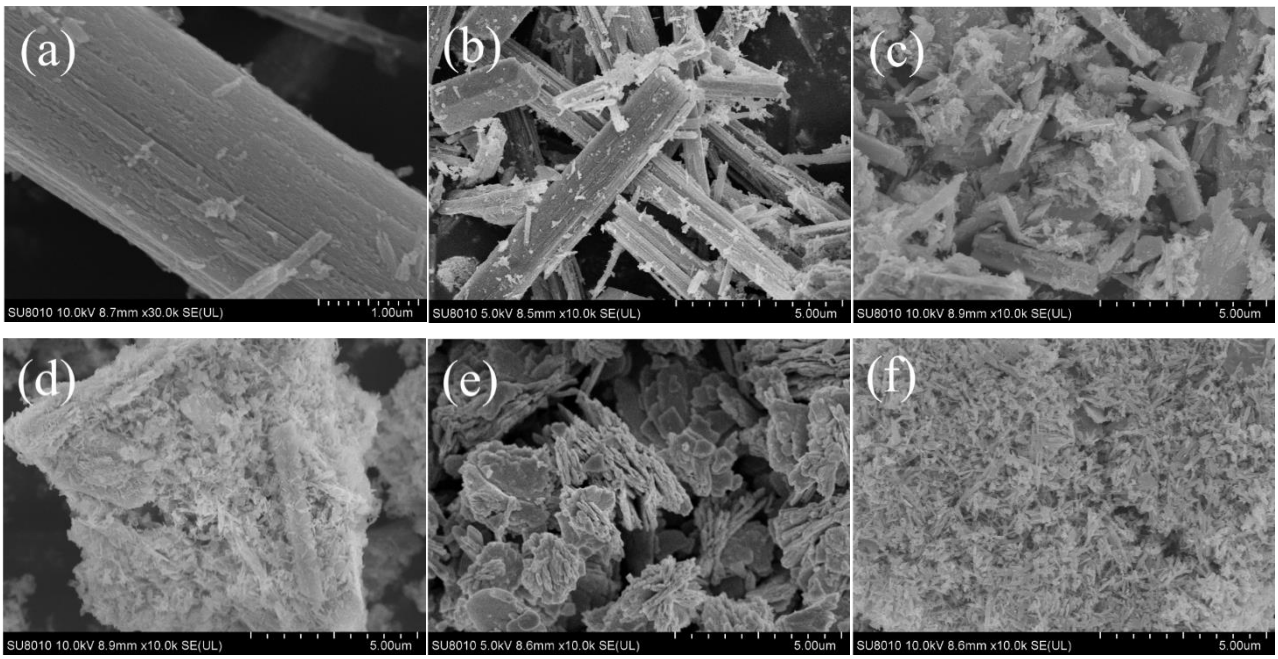

Fig. S3 FE-SEM images of (a) V/S-BiOI-3, (b) V/S-BiOI-1, (c) V/S-BiOI-2, (d) V/S-BiOI-4, (e) V/BiOI, and (f) S/BiOI

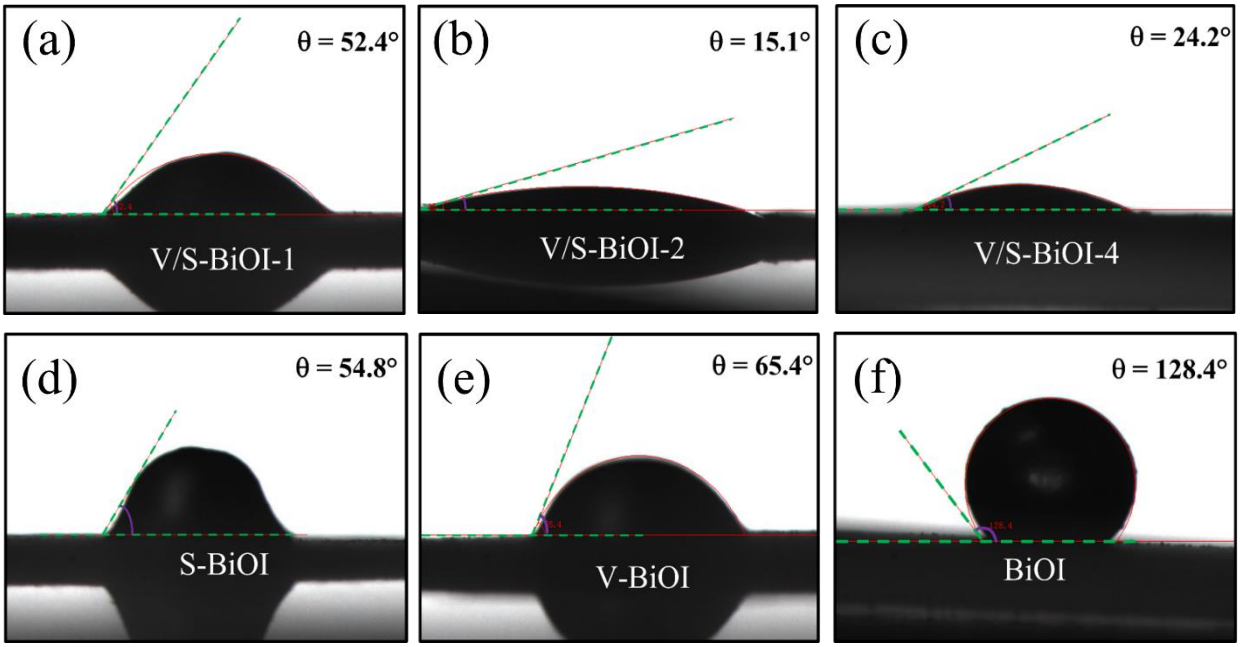

Fig. S4 Contact angle of (a) V/S-BiOI-1, (b) V/S-BiOI-2, (c) V/BiOI-4, (d) S-BiOI, (e) V/BiOI, and (f) BiOI.

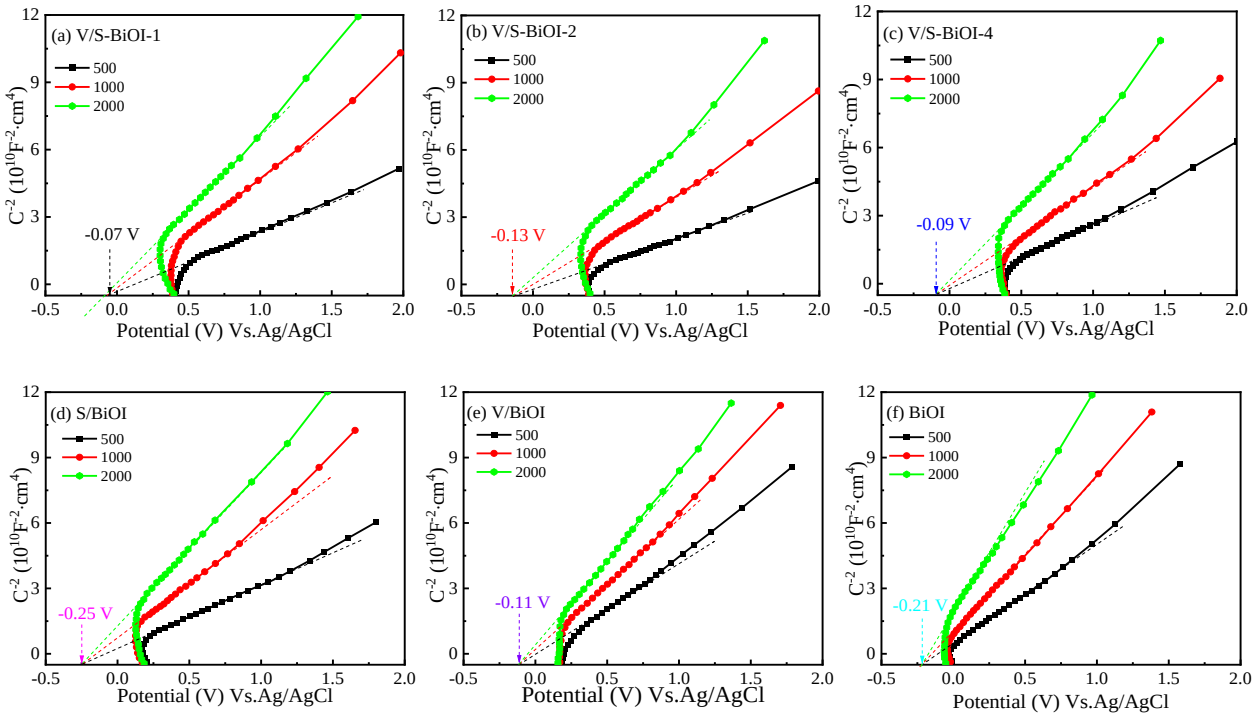

Fig. S5 Mott-Schottky curves of (a) V/S-BiOI-1, (b) V/S-BiOI-2, (c) V/S-BiOI-4, (d) S/BiOI, (e) V/BiOI, and (f) BiOI.

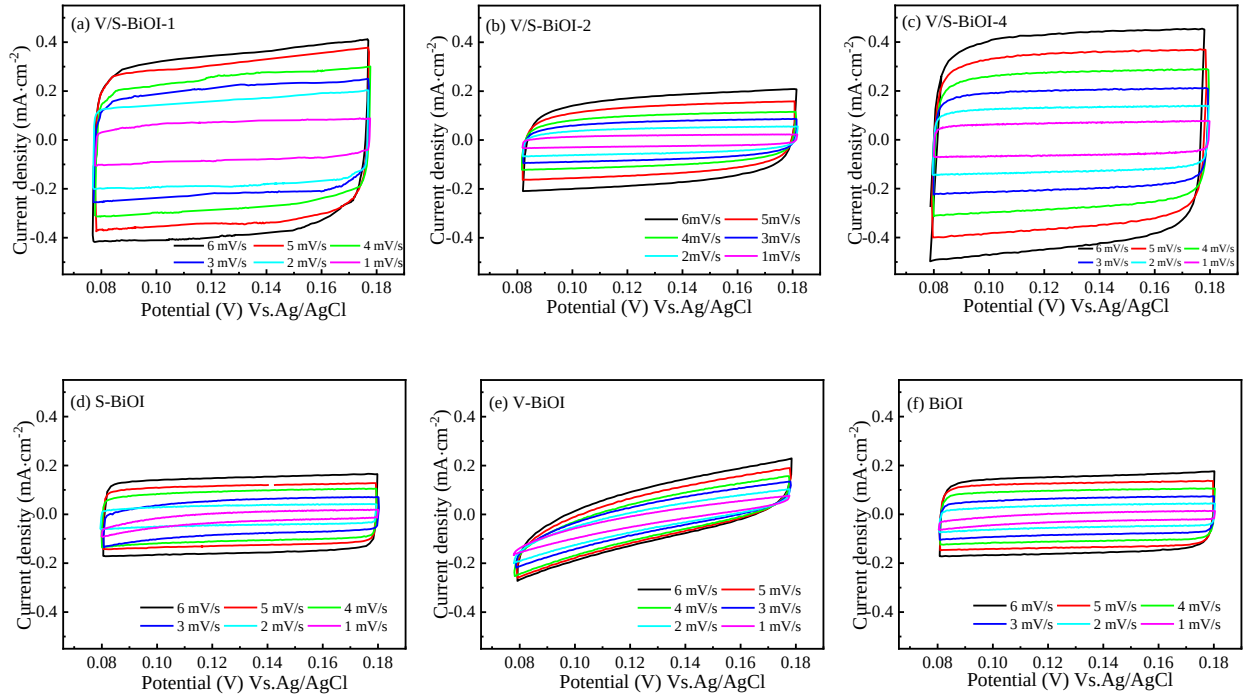

Fig. S6 CV tests of (a) V/S-BiOI-1, (b) V/S-BiOI-2, (c) V/S-BiOI-4, (d) S/BiOI, (e) V/BiOI, and (f) BiOI.

3. Additional Tables

Table S1 XPS element composition, crystal, and S_{BET} of V/S-BiOI, V-BiOI, S-BiOI, and BiOI

Catalyst	Atomic percentage/%					$V^{4+}/V^{4+}+V^{5+}$ (%)	Vo (%)	Crystallinity (%)	Crystal size (nm)	S_{BET} ($m^2 \cdot g^{-1}$)	Pore Volume ($cm^3 \cdot g^{-1}$)
	Bi	V	S	I	O						
V/S-BiOI-1	28.42	4.53	7.54	21.95	37.56	13.64	6.37	90.75	25.2	15.5	0.053
V/S-BiOI-2	27.22	5.77	7.75	21.86	37.40	17.82	14.75	89.67	22.6	15.6	0.059
V/S-BiOI-3	26.09	6.95	7.64	22.07	37.25	21.77	22.70	88.74	20.5	17.0	0.078
V/S-BiOI-4	25.92	7.68	7.79	21.47	37.14	25.73	9.86	85.42	22.9	15.8	0.062
V-BiOI	32.76	6.89	N/A	22.35	38.00	27.98	N/A	91.27	70.5	10.3	0.036
S-BiOI	32.59	N/A	7.48	22.66	37.27	N/A	N/A	91.54	70.8	10.2	0.039
BiOI	33.41	N/A	N/A	31.27	34.42	N/A	N/A	93.79	72.4	7.0	0.020

Table S2 Element contents from SEM-EDS analysis for V/S-BiOI, V-BiOI, S-BiOI, and BiOI

Catalyst	Bi	V	S	I	O
V/S-BiOI-1	28.32	4.64	7.41	21.71	37.92
V/S-BiOI-2	27.17	5.82	7.67	21.59	37. 75
V/S-BiOI-3	26.02	6.95	7.54	22.13	37.72
V/S-BiOI-4	25.87	7.37	7.65	21.98	37.13
V-BiOI	32.78	6.79	N/A	22.47	37.96
S-BiOI	32.62	N/A	7.38	22.84	37.16
BiOI	33.46	N/A	N/A	32.35	34.19

Table S3 XRF chemical element compositions of V/S-BiOI, V-BiOI, S-BiOI, and BiOI

Catalyst	Bi	V	S	I	O
V/S-BiOI-1	28.34	4.62	7.17	21.86	38.01
V/S-BiOI-2	27.22	5.67	7.53	21.71	37.87
V/S-BiOI-3	25.99	7.02	7.46	22.37	37.16
V/S-BiOI-4	25.83	7.42	7.51	22.13	37.11
V-BiOI	32.81	6.84	N/A	22.72	37.63
S-BiOI	32.65	N/A	7.31	23.06	36.98
BiOI	33.49	N/A	N/A	33.26	33.25

Table S4 Reports on PHER performance over bismuth oxyhalide catalysts

Catalyst	Sacrificial agent	Light source	AQE (%)	PHER rate ($mmol \cdot g^{-1} \cdot h^{-1}$)	Reference
$BiOCl/TiO_2$	Na_2S/Na_2SO_3	Visible light	N/A	1.355	[2]
$BiOI@ZnIn_2S_4$	TEOA	Visible light	8.7	4.03	[3]
GeSe/BiOI	Na_2S/Na_2SO_3	300 W Xe lamp	12.8	18.2	[4]
$BiOBr/BiVO_4$	Lactic acid	300 W Xe lamp	8.2	15.6	[5]
$BiOBr/Bi_2S_3$	Lactic acid	300 W Xe lamp	10.5	22.8	[6]
$TiO_{2-x}/BiOI$	Ethanol solution	AM 1.5G	4.46	0.804	[7]
W/S-BiOI	Na_2S /Na_2SO_3	300 W Xe lamp	N/A	0.723	[8]
$BiOI/Bi_2WO_6$	Furfural, n-butanol	500 W Xe lamp	N/A	2.22	[9]
GO/BiOCl	Methanol	45 W Philips lamp	17.97	0.34	[10]
Mn/S-BiOCl	Na_2S/Na_2SO_3	300 W Xe lamp	11.6	12.15	[11]
$Bi@O_V$-$BiOBr/Cu_3P$	Na_2SO_3 /KOH	Visible light	N/A	0.723	[12]
BiOBr/TpBD-COF	Ascorbic acid	300 W Xe lamp	0.34	16.17	[13]
OV-$BiOBr/Ni_2P$	KOH	Visible light	N/A	0.455	[14]
OV-$BiOBr/Cu_{2-x}S$	Na_2SO_3 /KOH	Visible light	N/A	0.509	[15]
V/S-BiOI	Na_2S/Na_2SO_3	300 W Xe lamp	12.9	25.25	This work

Table S5 The PHER rates, Vo (%), and contact angle (°) of catalysts

	V/S-BiOI-1	V/S-BiOI-2	V/S-BiOI-3	V/S-BiOI-4	V-BiOI	S-BiOI	BiOI
H_2 ($mmol \cdot g^{-1} \cdot h^{-1}$)	1.39	10.63	25.25	3.96	1.13	0	0
$V^{4+}/(V^{4+}+V^{5+})$ (%)	13.64	17.82	21.77	25.73	27.98	0	0
Vo (%)	6.37	14.75	23.49	9.86	0	0	0
Contact angle (°)	52.4	15.1	5.5	24.2	65.4	54.8	128.4

References:

[1] Q. Huang, Y. Xiong, Q. Zhang, H. Yao, Z. Li, Noble metal-free MoS_2 modified $Mn_{0.25}Cd_{0.75}S$ for highly efficient visible-light driven photocatalytic H_2 evolution. *Appl. Catal. B-Environ.*, 209 (2017) 514–522.

[2] R. Hou, M. Xu, Z. Fan, R. Zhong, Y. Xie, Y. Ling, Wang, BiOCl modified TiO_2 based catalyst with enhanced hydrogen generation properties under visible light via promote photogenerated electron-hole separation. *Mater. Today Phys.*, 44 (2024)101426.

[3] Y. Shen, J. Shi, J. Lei, P. Shan, A. Bian, W. Kong, W. Shi, Balls-on-ball structured S-scheme heterojunction with localized hotspot effects for boosted photothermal-assisted photocatalytic synthesis of hydrogen. *Chem. Eng. J.*, 508 (2025) 161072.

[4] N. Luo, W. Tang, B. Wang, H. Yuan, H. Chen, Engineering bilayer GeSe/BiOI S-scheme heterojunction for solar-driven water-splitting hydrogen evolution. *Int. J. Hydrogen Energ.*, 127 (2025) 521-529.

[5] R. Li, J. Peng, F. Xie, Q. Xi, J. Qin, H. Li, X. Yue, Construction of BiOBr/$BiVO_4$ S-scheme heterojunctions photocatalyst for efficient oxygen evolution from water splitting. *J. Environ. Chem. Eng.*, 13 (2025) 119738.

[6] J. Ma, L. Xu, Z. Yin, Z. Li, X. Dong, Z. Song, Y. Li, “One stone four birds” design atom co-sharing BiOBr/Bi_2S_3 S-scheme heterojunction photothermal synergistic enhanced full-spectrum photocatalytic activity. *Appl. Catal. B-Environ.*, 344 (2024) 123601.

[7] B. Zhang, D. Wang, S. Jiao, Z. Xu, Y. Liu, C. Zhao, J. Wang, TiO_{2-x} mesoporous nanospheres/BiOI nanosheets S-scheme heterostructure for high efficiency, stable and unbiased photocatalytic hydrogen production. *Chem. Eng. J.*, 446 (2022) 137138.

[8] Z. Su, C. Ye, Y. Xu, B. Wu, D.-H. Kuo, X. Wu, X. Chen, Synergistic vacancy defects and the surface hydrophobic-to-superhydrophilic wetting engineering in W/S co-doped BiOI for enhanced photocatalytic hydrogen evolution. *Chem. Eng. J.*, 496 (2024) 154282.

[9] Y. Qu, K. Bu, J. Zhang, D. Chen, H. Li, L. Bai, Advancing Z-scheme BiOI/Bi_2WO_6 photocatalysts for the acetalization of furfural and H_2 evolution in fatty alcohols under the visible light. *Renew. Energ.*, 247 (2025) 123045.

[10] P. Hait, R. Mehta, S. Basu, Advancing sustainable solutions: harnessing polya-niline/BiOCl/GO ternary nanocomposites for solar-powered degradation of organic pollutant and photocatalytic hydrogen generation. *J. Clean. Prod.*, 424 (2023) 138851.

[11] Z. Su, B. Wu, C. Li, D. Kuo, P. Zhang, L. Chen, D. Lu, J. Lin, X. Chen, Z. Yuan, Mn/S co-doped BiOCl regulated with a hydrophobic-to-superhydrophilic transition and oxygen-vacancy defects for assisting photocatalytic hydrogen evolution. *Chem. Eng. J.*, 510 (2025) 161621.

[12] X. Li, T. Han, Y. Zhou, M. Wang, Z. Tian, F. Deng, Y. Luo, Y. Xie, J. Huang, L. Han, Z. Chen, Z. Feng, W. Chen, Boosting photoelectrocatalytic hydrogen evolution of Bi@OV-BiOBr/Cu_3P high-low heterojunction with dual-channel charge transfer. *Appl. Catal. B-Environ.*, 350 (2024) 123913.

[13] H. Ran, X. Liu, J. Fan, Y. Yang, L. Zhang, Q. Guo, B. Zhu, Q. Xu, Engineering BiOBr/TpBD-COF S-scheme heterointerface via phase transformation strategy for boosted photocatalytic hydrogen generation. *J. Materiomics*, 11 (2025) 100918.

[14] X. Li, Y. Hu, F. Dong, J. Huang, L. Han, F. Deng, Y. Luo, Y. Xie, C. He, Z. Feng, Z. Chen, Y. Zhu, Non-noble-metallic Ni_2P nanoparticles modified O_V-BiOBr with boosting photoelectrochemical hydrogen evolution without sacrificial agent. *Appl. Catal. B-Environ.*, 325 (2023) 122341.

[15] X. Li, Q. Liu, F. Deng, J. Huang, L. Han, C. He, Z. Chen,Y. Luo, Y. Zhu, Double-defect-induced polarization enhanced OV-BiOBr/$Cu_{2-x}S$ high-low junction for boosted photoelectrochemical hydrogen evolution. *Appl. Catal. B-Environ.*, 314 (2022) 121502.